Spectroscopy and dynamics of methylamine. II. Rotational and vibrational structures of CH_3NH_2 and CH_3ND_2 in cationic D_0 states

Sun Jong Baek, Kyo-Won Choi, and Young S. Choi
Department of Chemistry, Inha University, Incheon (402-751), Republic of Korea

Sang Kyu Kim[a)]
Department of Chemistry, Inha University, Incheon (402-751), Republic of Korea and Department of Chemistry and School of Molecular Sciences, Korea Advanced Institute of Science and Technology (KAIST), Daejeon (305-701), Republic of Korea

(Received 16 December 2002; accepted 27 March 2003)

Accurate and precise ionization energies of methylamines (CH_3NH_2 and CH_3ND_2) are determined to be 9.0422 ± 0.0012 and 9.0532 ± 0.0012 eV, respectively, by $(1+1')$ two-photon mass-analyzed threshold ionization (MATI) spectroscopy. From selective ionizations from specified intermediate quantum states, fundamental frequencies of amino-wagging and CH_3-rocking modes of $CH_3NH_2^+$ ($CH_3ND_2^+$) in D_0 states are determined to be 738 (573) and 1013 (1024) cm^{-1}, respectively. The frequency of the amino wag is largely blueshifted from that of the neutral S_1 state, while the CH_3-rocking frequency is little shifted from that of S_1. Internal rotational constants associated with the nearly free internal rotation of the top (amino group) with respect to the frame (methyl group) about the C–N axis are accurately determined, from which the geometries of methylamine ions are revealed. Barrier heights for torsional motion in $CH_3ND_2^+$ are determined to be 25 ± 5 and 34 ± 5 cm^{-1} at the origin and first ND_2-wagging bands, respectively. Mode-resolved spectroscopy using the MATI signal for resolving overlapped spectral features in the intermediate state is employed for clarifying the vibrational assignment of the intermediate state. An *ab initio* calculation at the QCISD level is carried out, giving good agreement with the experiment. © *2003 American Institute of Physics.* [DOI: 10.1063/1.1575735]

I. INTRODUCTION

As a primary amine, methylamine is a very important molecule in organic syntheses and biological processes. Thermodynamic properties such as basicity and proton affinity of methylamine are main factors in determining its organic reactivity as a Lewis base.[1–5] Especially, comparison among basicities or proton affinities of many primary, secondary, and tertiary amines is very important in understanding not only their own chemistry, but also charge donating and withdrawing effects of various substituents. Accordingly, gas-phase basicities and proton affinities of various aliphatic amines have been extensively measured.[1,5] Ionization potentials of various amines were also determined by extensive photoelectron spectroscopic studies, since those are closely related to corresponding proton affinities or hydrogen atom affinities.[6] However, for example, the photoelectron spectra of methylamine using He(I) or synchrotron radiation consist of broadbands at the electron kinetic energy near the ionization threshold region.[6,7] Thus ionization energies of amines determined by conventional photoelectron spectroscopy have relatively large uncertainties.[6] A more accurate and precise measurement of the ionization potentials of methylamine and related compounds would lead to a more accurate quantitative description of the thermodynamic properties of such important compounds.

Relatively recently developed zero-electron kinetic energy (ZEKE) or mass-analyzed threshold ionization (MATI) spectroscopy has served as an excellent method for accurate measurement of ionization potentials with a precision of ±0.1 cm^{-1}.[1,8–22] No such ZEKE or MATI spectroscopy had been done yet for any aliphatic amine, though it was carried out for some of the aryl amines such as aniline and 2-aminopyridine.[19–22] In this work, the first measurement of accurate ionization potentials of methylamines, CH_3NH_2 and CH_3ND_2, is reported with vibrational frequencies of cations. In the preceding paper,[23] rovibrational structures of methylamines (CH_3NH_2 and CH_3ND_2) in neutral S_1 states were revealed by $(1+1)$ resonant-enhanced two-photon ionization (R2PI) spectroscopy. Accordingly, rovibrational structures of methylamines in neutral excited ($\tilde{A}$) and ground cationic (D_0) states are also compared here. *Ab initio* calculations for the ground cationic methylamines are also presented to be compared with the experiment.

II. EXPERIMENT

Sampling conditions are identical to those described in the preceding paper.[23] Briefly, CH_3NH_2 and CH_3ND_2 were purchased (Aldrich) and synthesized, respectively, by the method described earlier.[23] Methylamine in neon gas was expanded through a 0.3-mm-diam nozzle orifice (General Valve) with a backing pressure of ~3.5 atm and a repetition rate of 10 Hz before it was skimmed through a 1-mm-diam skimmer (Precision Instrument Services). Background pres-

a)Author to whom correspondence should be addressed. Electronic mail: skkim@inha.ac.kr

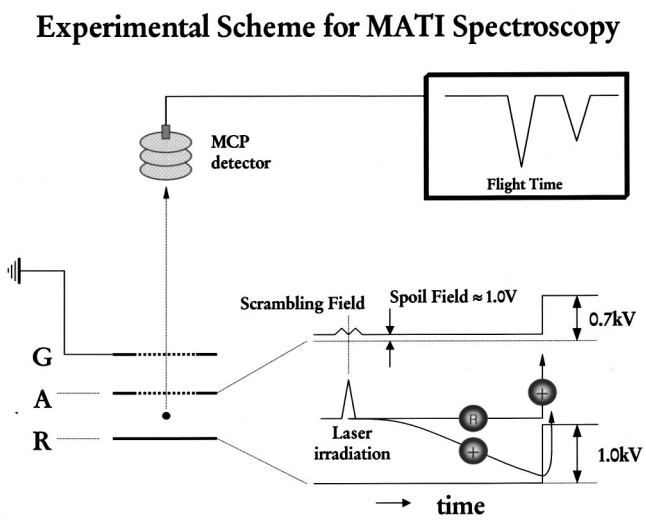

FIG. 1. Experimental setup for MATI spectroscopy. Directly formed ions and MATI ions are separated in time by applying a spoil field before pulsed-field ionization of MATI states.

sures were maintained at $\sim 10^{-5}$ and $\sim 10^{-7}$ Torr for source and ionization chambers, respectively, when the nozzle was operated. The 355-nm output of a Nd:YAG laser (Spectra-Physics, GCR-150, 10 Hz) was used to pump a dye laser (Lambda-Physik, Scanmate II) to generate laser pulses in the 440–480 nm range. The laser output was then frequency doubled in a BBO crystal placed on an autotracker to generate tunable UV laser pulses with a 0.25-cm^{-1} spectral bandwidth in the 220–240 nm region. The other laser pulse (3–4 mJ/pulse, 6 ns) was generated in the 300–320 nm region via doubling the laser output from the other dye laser (Lumonics, HD500) pumped by the 532-nm output of the other Nd:YAG laser (Continuum Surelite-II). Frequency doubling was made on a KD*P crystal placed on another homemade autotracker to maintain both the intensity and direction of the laser beam while its wavelength was scanning. Two independently tunable laser pulses were then spatially and temporally overlapped and crossed the molecular beam in a counterpropagation manner.

Molecules excited to long-lived high-n,l Rydberg states via two independently tunable laser pulses at resonance wavelengths were allowed to stay for 5–10 μs in the presence of a spoil field of $\sim$0.2 V/cm and ionized by applying a pulsed electric field of 20–400 V/cm, Fig. 1. MATI ions were then accelerated, drifted along the field-free region, detected by dual microchannel plates (MCP, Jordan), digitized by an oscilloscope (LeCroy MODEL), and stored in a personal computer, which also controlled two dye lasers and autotrackers. In the presence of the spoil field, directly formed ions were separated out in time along the time-of-flight axis, Fig. 1. To enhance the MATI signal, a scrambling field was applied at the moment of laser excitation. Absolute frequencies of dye laser outputs were calibrated within an accuracy of ± 0.5 cm^{-1} using the optogalvanic effect in an iron hollow-cathode lamp with Ne gas.

III. RESULTS AND DISCUSSION

An internal-rotor Hamiltonian with a sixfold sinusoidal potential function was quite successfully applied in the interpretation of excitation spectra of CH_3NH_2 and CH_3ND_2 in the preceding paper.[23] The same Hamiltonian is used here for the interpretation of MATI spectra. However, it should be noted that selection rules for the $D_0-\tilde{A}$ transition are different from those for the $\tilde{A}-X$ transition. Namely, since the $3s$ orbital belongs to A_1' in G_{12} (CNPI) group, a removal of the $3s$ electron does not alter the symmetry of the electronic state. From the symmetry requirement, such a transition is induced by the totally symmetric (A_1') transition dipole moment. Accordingly, the transition dipole moment in the $D_0-\tilde{A}$ transition is along the molecular a axis, giving an a-type transition with rotational selection rules of $\Delta|K|=0$ and $\Delta J=0,\pm 1$. Nuclear spin wave functions are conserved. Symmetry species of internal-rotor states are to be conserved also in the ionization from intermediate states, giving a selection rule of $\Delta m=0$. These symmetry selection rules are applied in the simulation of MATI spectra.

It is well known that ionization energies deduced from MATI peak positions are slightly below true ionization energies.[8] This is due to the presence of an electric field in the moment of the ionization event. The origin MATI band in the $D_0-\tilde{A}$ transition is taken at several values of the pulsed-field (F) in the 20–500 V/cm range. MATI peak positions are plotted versus the square root of F, and a best-fitted straight line is extrapolated to give the MATI peak position at zero electric field. Absolute ionization energies are calibrated accordingly.

A. $CH_3ND_2^+(D_0)$

The origin band spectrum for the $\tilde{A}-X$ transition in the preceding paper[23] is located at the bottom in Fig. 2. MATI bands excited via intermediate states with different overall and internal rotational quantum numbers are shown with appropriate labels connecting intermediate levels to their associated MATI spectra, Fig. 2. It should be noted that MATI bands are intrinsically broad due to the pulsed-field ionization scheme.[8] The full width at half maximum of an individual MATI peak is estimated to be around 4 cm^{-1}. Because of the severe selection rule of $\Delta|K|=0$, $\Delta J=0,\pm 1$, and $\Delta m=0$ (*vide supra*), only a few MATI bands carry significant intensities in each spectrum. Using the Hamiltonian described in the preceding paper combined with appropriate selection rules,[23] the simulation is carried out as shown in Fig. 2. For instance, the MATI spectrum "b" in Fig. 2 represents cationic energy levels ionized via intermediate states of $(K',m')=(1,-1)$, $(-1,1)$, or $(\pm 1,\pm 2)$. From selection rules, symmetry-allowed cationic energy levels from those intermediate states are states with quantum numbers (K^+,m^+) of $(1,-1)$, $(-1,-1)$, $(-1,1)$, $(1,1)$, $(1,2)$, $(-1,2)$, $(1,-2)$, or $(-1,-2)$. Energetically accessible J^+ states are also included in the simulation with the selection rule of $\Delta J=0,\pm 1$. Accordingly, the simulation predicts three major MATI peaks in the "b" MATI spectrum in Fig. 2, and it seems to match the experiment quite well though relative peak intensities of the experiment and simulation are not

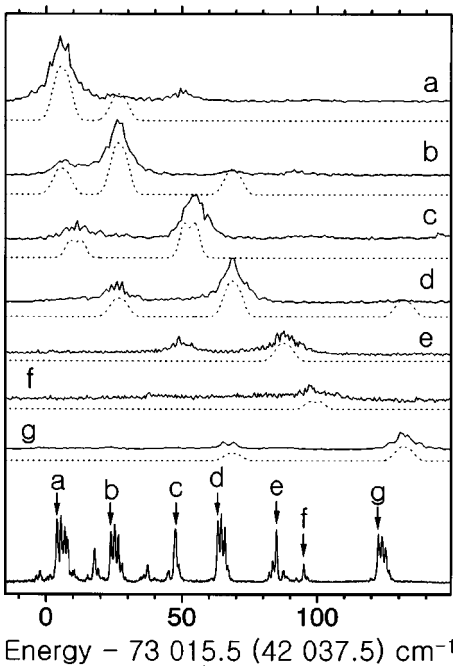

FIG. 2. MATI spectra of $CH_3ND_2^+$ taken via various intermediate states of the origin band in the R2PI spectrum (Ref. 23). Excited states labeled with arrows in the R2PI spectrum are used as intermediate states in the $(1+1')$ MATI excitation to give associated MATI spectra. Simulations (dotted traces) based on parameters in Table I are shown together. The total energy for the MATI excitation is shown on the abscissa, while the excitation energy to the intermediate state is shown in parentheses.

perfectly reproduced. Parameters used in simulations in Fig. 2 are listed in Table I. The $D_0-\tilde{A}$ origin is accurately determined to be 30 981 cm^{-1}, giving an adiabatic CH_3ND_2 ionization energy (IE) of $73\,019\pm10$ cm^{-1} (IE$=9.0532\pm0.0012$ eV) considering the $\tilde{A}-X$ origin$=42\,038$ cm^{-1}.[23] Internal rotational constants of the top (ND_2) and frame (CH_3) are determined to be identical to give $A^{T+}=A^{F+}=5.25\,cm^{-1}$. The corresponding moment of inertia is 3.21 amu Å^2. This is larger than the A^T or A^F value of 4.93 cm^{-1} of $CH_3ND_2(\tilde{A})$ at the zero-point energy level, indicating that the angle of D–N–D, for instance, tends to be smaller in the cation compared to that of $CH_3ND_2(\tilde{A})$. The overall rotational constant B^+ could not be accurately determined in the simulation due to the broad MATI linewidth. MATI peak positions via intermediate states labeled as "e" and "f" in Fig. 2 are very sensitive to a barrier height (V_6^+) for internal rotation of ND_2 with respect to CH_3 in the $CH_3ND_2^+(D_0)$. The simulation matches the experiment when $V_6^+=25\pm5$ cm^{-1} in Fig. 2. *Ab initio* [QCISD, 6-31+G9(d)] geometries of the planar and ciscoid forms of $CH_3NH_2^+$ are shown with their calculated

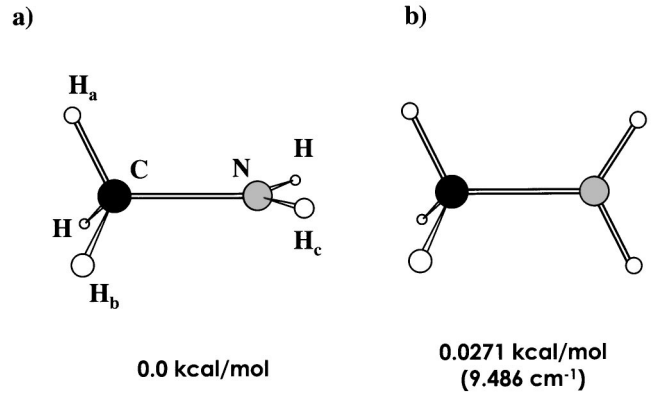

FIG. 3. Geometries of $CH_3NH_2^+$ calculated by *ab initio* calculation at the QCISD level with a 6−31G+(d) basis set. Methylamine cation in (a) planar geometry is predicted to be slightly more stable than (b) ciscoid geometry. Relative stabilization energies in cm^{-1} are shown.

relative stabilization energies of 0 and 9.8 cm^{-1}, respectively, in Fig. 3. This energy difference is in good agreement with the experiment, especially since V_6^+ is expected to be even lower at the potential minimum.

MATI spectra taken via the first ND_2-wagging band of $CH_3ND_2(\tilde{A})$ show spectral features similar to those taken via the origin band. However, as clearly shown in Fig. 4, MATI peak positions are all blueshifted from associated R2PI peak positions in terms of their internal energies, indicating that the ND_2-wagging frequency (ν_9^+) becomes higher in the cation compared to that of the neutral excited state. Simulations are carried out for precise determination of internal rotational constants and vibrational frequency in Fig. 5. The fundamental frequency of the ND_2 wag of $CH_3ND_2^+$ is determined to be 573 cm^{-1}. This is a large shift from the ND_2-wagging frequency of 487 cm^{-1} in $CH_3ND_2(\tilde{A})$, suggesting that the removal of the $3s$ electron modifies the potential energy surface along the amino-wagging motion quite significantly. Internal rotational constants are determined to give $A^{T+}(v^+=1)=A^{F+}(v^+=1)=5.06\,cm^{-1}$. This is decreased from the value of 5.25 cm^{-1} in the origin band. From the simple equation of $A^{T+}(v^+)=A_e^{T+}-\alpha_e^+(v^++\frac{1}{2})$, it is found that $A_e^{T+}=A_e^{F+}=5.35\,cm^{-1}$, while $\alpha_e^+=0.19\,cm^{-1}$. The value of α_e^+, a measure of interaction between internal rotation and ND_2 wag, is larger than that of neutral excited state.[23] This could be partly due to the more effective coupling caused by the faster internal rotation of $CH_3ND_2^+$ due to its lower moment of inertia compared to that of $CH_3ND_2(\tilde{A})$. The torsional barrier height at the first ND_2-wag level is determined to be 34 ± 5 cm^{-1} in the simulation, Fig. 5. Similar to the case of $CH_3ND_2(\tilde{A})$, the torsional barrier increases when

TABLE I. Molecular constants used in the simulations for $CH_3ND_2^+$ MATI spectra.

	Origin	ν_9^+	ν_7^+	$2\nu_9^+$	$\nu_7^++\nu_9^+$	$3\nu_9^+$	$\nu_7^++2\nu_9^+$	$4\nu_9^+$
A^{T+}	5.25±0.05	5.06±0.05						
A^{F+}	5.25±0.05	5.06±0.05						
B^+	(0.7)	(0.7)						
V_6^+	25±5	34±5						
E_{vib}^+	0[+73019]	573±1	1024±1	1155±2	1621±2	1713±5	2217±2	2270±5

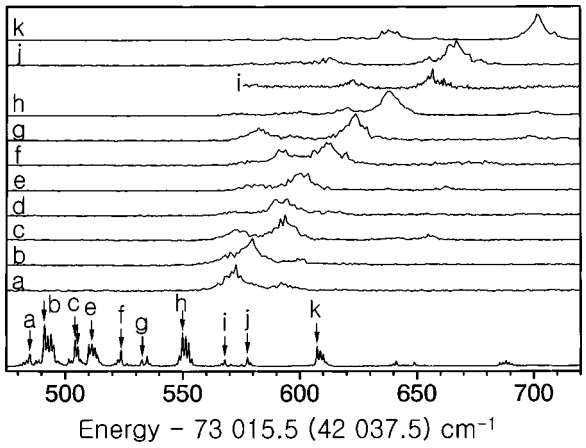

FIG. 4. MATI spectra of $CH_3ND_2^+$ taken via various intermediate states of the first ND_2-wag band in the R2PI spectrum (Ref. 23). See the caption in Fig. 2.

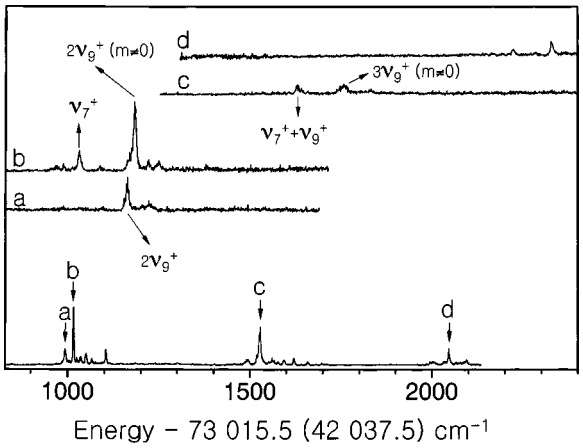

FIG. 6. MATI spectra of $CH_3ND_2^+$ taken via various intermediate states with internal energies above ~1000 cm^{-1} (Ref. 23). Excited states labeled with arrows in the R2PI spectrum are used as intermediate states in the $(1+1')$ MATI excitation to give associated MATI spectra. The total energy for the MATI excitation is shown on the abscissa, while the excitation energy to the intermediate state is shown in parentheses. Assignments of MATI bands are appropriately denoted.

torsional motion is combined with one quantum of ND_2 wag. Prediction of this value with a Hamiltonian including ND_2-wag–torsion coupling would be a very interesting theoretical work.

As described in the preceding paper,[23] homogeneous line broadening becomes severe in intermediate states at internal energies higher than ~1000 cm^{-1}, and thus selection of a specific rotational intermediate state in the MATI scheme is not plausible. MATI spectra are taken via just a few intermediate S_1 bands. In Fig. 6, the R2PI spectrum at internal energies higher than ~1000 cm^{-1} is shown at the bottom, while MATI spectra are appropriately labeled according to S_1 states used as intermediate states in the ionization scheme. The MATI spectrum "a," taken via the bandhead of $2\nu_9(\tilde{A})$, shows a single main MATI band representing the $2\nu_9^+$ band of $CH_3ND_2^+$. From the MATI peak position in the "a" spectrum in Fig. 6, the vibrational term value is determined to be 1155 cm^{-1} for $2\nu_9^+$. Now, using the simple equation of $E_{\mathrm{vib}}^+(v^+) = \omega_e^+(v^+ + \frac{1}{2}) + \chi_{99}^+(v^+ + \frac{1}{2})^2$ and fundamental and first overtone frequencies of ND_2 wag, it is found that $\omega_e^+ = 564\,\mathrm{cm}^{-1}$ and $\chi_{99}^+ = 4.5\,\mathrm{cm}^{-1}$.

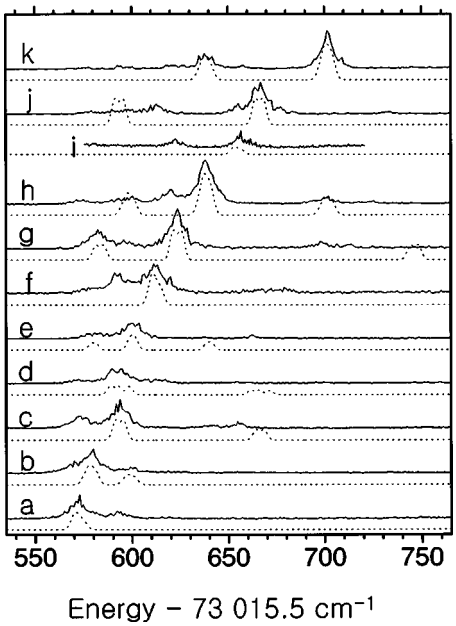

FIG. 5. MATI spectra identical to those in Fig. 4 with simulations carried out based on parameters in Table I.

The most interesting spectral feature is found in the MATI spectrum "b" in Fig. 6. The peak labeled as "b" in the R2PI spectrum is actually due to two different modes ν_7 and $2\nu_9$. These two overlapped bands are very well separated in the MATI spectrum. That is, in the MATI spectrum it is found that vibrational energies of ν_7^+ and $2\nu_9^+$ are quite distinct, giving their respective vibrational energies of 1024 and 1155 cm^{-1}. The shift of the second peak position in the "b" MATI spectrum from the main peak position in the "a" MATI spectrum is due to the higher internal-rotational energy of the former. The difference in magnitudes of vibrational frequency changes upon ionization for different modes is extremely useful to resolve overlapped intermediate states. In this case, a mode-resolved spectroscopic technique, which was introduced in Ref. 19, is quite useful to identify spectral bands due to a specific mode from overlapped bands contributed from two or more different modes. In the mode-resolved spectroscopy, the MATI signal is monitored while the first excitation energy to intermediate states is varied. That is, the energy for the D_0–$\tilde{A}$ transition is fixed either at 30 993 =origin of $(D_0-\tilde{A})+1024-1012$ or 31 145=origin of $(D_0-\tilde{A})+1176-1012\,\mathrm{cm}^{-1}$. And then the excitation energy for the $\tilde{A}$–X transition is varied to give two distinct mode-resolved spectra for the intermediate $\tilde{A}$ state as shown Fig. 7. For comparison, the $\tilde{A}$–X R2PI spectrum of CH_3ND_2 in the same energy region[23] is also shown in Fig. 7(a). In this way, intermediate states of modes having the largest Franck–Condon factors with either the $1024(\nu_7^+)$ or $1176(2\nu_9^+)\,\mathrm{cm}^{-1}$ band are separated out in two distinct mode-resolved spectra in Figs. 7(b) and 7(c), respectively. Peak intensities are related to Franck–Condon factors and

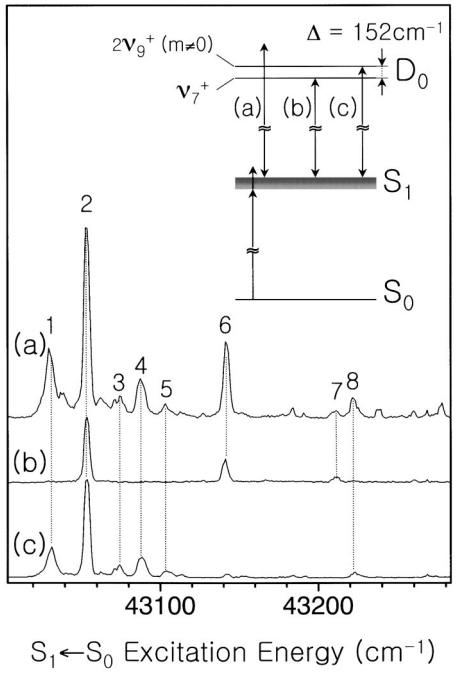

FIG. 7. (a) R2PI spectrum of $CH_3ND_2^+$ in the 43 000–43 280 cm^{-1} region. Mode-resolved spectra taken with a fixed ionization energy of (b) 30 993 or (c) 31 145 cm^{-1} to reach ν_7^+ or $2\nu_9^+$ level, respectively. In mode-resolved spectra, the MATI signal is monitored while the S_1-S_0 excitation energy is scanned.

selection rules involved in both $\tilde{A}-X$ and $D_0-\tilde{A}$ transitions, and they are not straightforward to be interpreted. However, peak positions are quite well described in the preceding paper.[23] Major peaks in the R2PI spectrum in Fig. 7(a) are labeled as 1–8. Since peak 2 is chosen to be an intermediate band for ionization, only peak 2 is expected to be divided into two bands belonging to either ν_7 or $2\nu_9$ in Fig. 7(b) or 7(c), respectively. Accordingly, most prominent peaks in mode-resolved spectra are at the peak-2 position. Because of broad experimental linewidths of $\tilde{A}-X$ and $D_0-\tilde{A}$ transitions, no difference is observed between two bands at the 2 position in two different mode-resolved spectra, in terms of position and linewidth except their different relative intensities. Although two bands in two different mode-resolved spectra look the same, these spectra nail down the fact that the 1024-cm^{-1} band in the R2PI spectrum (peak 2) is actually due to ν_7 and $2\nu_9$ modes, in which the higher internal-rotor quantum numbers are combined in the latter compared to those in the former.

A more intriguing experimental fact is that small peaks other than peak 2 are additionally observed in mode-resolved spectra in Figs. 7(b) and 7(c). Internal-rotor energy levels are similar in D_0 and $\tilde{A}$ states, and both $\tilde{A}-X$ and $D_0-\tilde{A}$ transitions carry broad linewidths. Therefore, excitation energies to peaks 1, 3, 4, 5, and 8 in the $\tilde{A}-X$ transition given in addition to a fixed $D_0-\tilde{A}$ transition energy of 31 145 cm^{-1} are nearly resonant with adjacent MATI states having almost the same internal-rotor energies as those of intermediate states associated with peaks 1, 3, 4, 5, and 8. Because bandheads of ν_7^+ and $2\nu_9^+$ are remote to each other with a energy difference of 151 cm^{-1}, it is not energetically accessible for excitations to ν_7 intermediate states to be resonant with ν_7^+ MATI states in the mode-resolved spectrum using the $2\nu_9^+$ MATI signal, Fig. 7(c). Therefore, the existence of additional 1, 3, 4, 5, and 8 peaks in Fig. 7(c) indicates that these peaks belong to the $2\nu_9$ band of the $\tilde{A}$ state. This is quite consistent with the band assignment made in the preceding paper.[23] The same logic applies to the mode-resolved spectrum using the ν_7^+ MATI signal in Fig. 7(b). Accordingly, peaks 6 and 7 most likely belong to the ν_7 band of the $\tilde{A}$ state, though the corresponding MATI signal is relatively weak. It is found, in the preceding paper,[23] that the lifetime associated with peak 6 is about the same as that associated with the ν_7 bandhead, giving a longer lifetime of the ν_7 band (~4 ps) compared to that of the isoenergetic $2\nu_9$ band (~1.8 ps).[23] This experimental fact is quite consistent with the above assignment. The mode-resolved spectroscopic technique employed here and introduced in Ref. 19 once again turns out to be extremely useful in assigning and identifying overlapped complex intermediate states in $(1+1')$ two-photon MATI spectroscopy.

The "c" MATI spectrum via the "c" R2PI band in Fig. 6 shows two main MATI bands due to $\nu_7^+ + \nu_9^+$ and $3\nu_9^+$ bands, in which the former represent its bandhead while the latter is combined with internal-rotor excitation. MATI peak positions provide vibrational energies of 1621 and 1713 cm^{-1} for $\nu_7^+ + \nu_9^+$ and $3\nu_9^+$ modes, respectively, Table I. The latter is slightly smaller than the value of 1746 cm^{-1} predicted from $\omega_e^+ = 564\,cm^{-1}$ and $\chi_{99}^+ = 4.5\,cm^{-1}$ (*vide supra*), while the former is a little bit larger than the value of 1596 cm^{-1}, which is the direct sum of fundamental frequencies of ν_7^+ and ν_9^+. Similarly, in the "d" MATI spectrum taken via the "d" R2PI band in Fig. 6, two main MATI bands due to $\nu_7^+ + 2\nu_9^+$ and $4\nu_9^+$ are observed, giving their respective vibrational energies of 2217 and 2270 cm^{-1}, Table I. Vacuum UV one-photon MATI spectroscopy would be very useful for exploring the higher-frequency vibrational modes.

B. $CH_3NH_2^+(D_0)$

The R2PI spectrum of CH_3NH_2 consists of broadbands due to ultrashort excited-state lifetimes.[23] Accordingly, selection of a specific rotational state as an intermediate state in the MATI ionization scheme is not plausible. However, by selecting the excitation energy, MATI spectra showing structures due to internal-rotor states are revealed. In Fig. 8, the R2PI origin band of CH_3NH_2 is shown at the bottom, and MATI spectra taken via various intermediate states are shown with appropriate labels connecting the intermediate band and its associated MATI spectrum. These MATI spectra are well reproduced by simulations (dotted traces in Fig. 8) using the parameters in Table II. The $D_0-\tilde{A}$ origin is accurately determined to be 31 261 cm^{-1}, when it is added to the $\tilde{A}-X$ origin of 41 669 cm^{-1}, giving an adiabatic CH_3NH_2 ionization energy of 72 930±10 cm^{-1} (IE=9.0422±0.0012 eV). This value is ~0.1 eV higher than the previously measured ionization potential of 8.9±0.1 eV (Refs. 1 and 6) and ~0.1 eV lower than the more recently reported value of 9.16 ±0.01 eV (Ref. 7). The former value is consistent with our

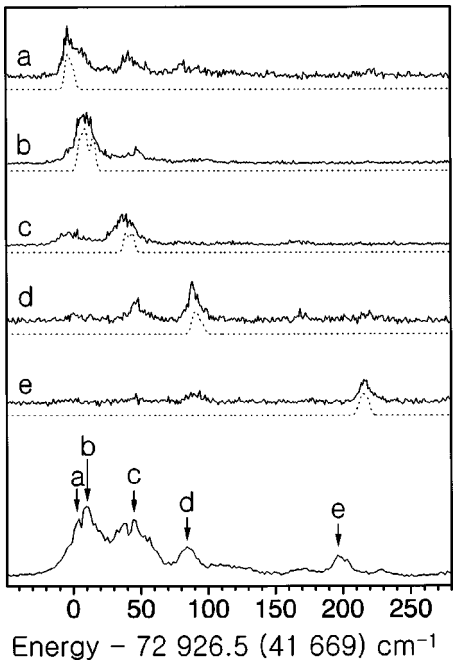

FIG. 8. MATI spectra of $CH_3NH_2^+$ taken via various intermediate states of the origin band in the R2PI spectrum (Ref. 23). See the caption in Fig. 2.

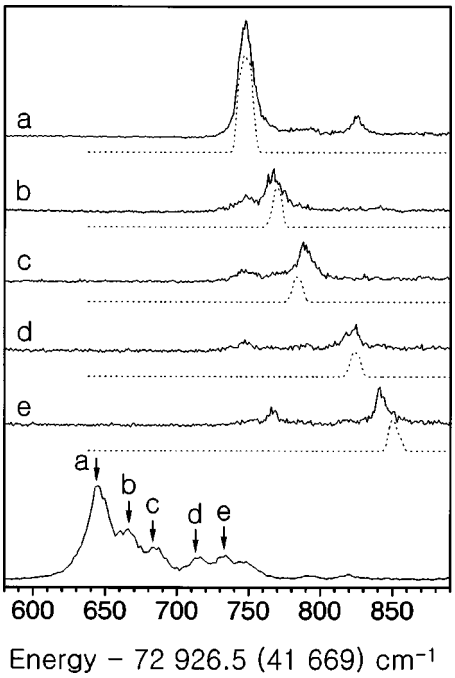

FIG. 9. MATI spectra of $CH_3NH_2^+$ taken via various intermediate states of the first NH_2-wag band in the R2PI spectrum (Ref. 23). See the caption in Fig. 2.

data within its error limits, while the latter is not. Poor characterization of the CH_3NH_2 intermediate state hampers accurate determination of other molecular constants such as A^{T+}, B^+, and V_6^+. The internal-rotational constant of the top (NH_2) is expected to be close to the double of that of the frame (CH_3) (Ref. 23) to give $A^{T+}=10.5\,cm^{-1}$ and $A^{F+}=5.25\,cm^{-1}$. Simulations using these internal rotational constants turn out to be in good agreement with experiments, Fig. 8.

MATI spectra taken via the first NH_2-wagging band of $CH_3NH_2(\tilde{A})$ show spectral features similar to those taken via the origin band, Fig. 9. Similarly to the case of CH_3ND_2, MATI peak positions of CH_3NH_2 are also quite blueshifted from associated R2PI peak positions in their internal energies. The fundamental frequency of the NH_2 wag of $CH_3NH_2^+$ is accurately determined to be 738 cm^{-1}. This is a large shift from the ND_2-wagging frequency of 636 cm^{-1} in $CH_3NH_2(\tilde{A})$. Internal-rotational constants used in the simulation are $A^{T+}(v^+=1)=10.12\,cm^{-1}$ and $A^{F+}(v^+=1)=5.06\,cm^{-1}$. In Fig. 10, the CH_3NH_2 R2PI spectrum at internal energies higher than ~1000 cm^{-1} is shown at the bottom with MATI spectra appropriately labeled according to S_1 intermediate states. The ν_7 band of $CH_3NH_2(\tilde{A})$ is well isolated in the R2PI spectrum. Therefore, the MATI spectrum "a," taken via the bandhead of $\nu_7(\tilde{A})$, shows a single main MATI band representing the ν_7^+ band of $CH_3NH_2^+$, Fig. 10. The fundamental frequency of ν_7^+ is determined to be 1013 cm^{-1}, and this is only slightly higher than that of $\nu_7(\tilde{A})=1008\,cm^{-1}$. From MATI spectra "b" and "c" in Fig. 10, the vibrational term value is determined to be 1475 cm^{-1} for $2\nu_9^+$. The analysis of MATI spectra "d"–"h" in Fig. 10 provides vibrational energies of 1749, 2020, and 2219 for $\nu_7^+ + \nu_9^+$, $2\nu_7^+$, and $3\nu_9^+$ modes, respectively, Table II.

C. *Ab initio* calculation and energetics

An *ab initio* calculation is carried out for methylamine ions at the QCISD level with a 6-31+G(d) basis set. Geometric parameters for the minimum planar structure are listed with calculated vibrational frequencies in Table III. Internal-rotational constants of $CH_3ND_2^+$ are calculated from the *ab initio* geometry to give $A^T=5.530\,cm^{-1}$ and $A^F=5.198\,cm^{-1}$. Interestingly, the average of these A^T and A^F values is 5.364 cm^{-1}, and this is very close to the experimental value of $A_e^T=A_e^F=5.35\,cm^{-1}$. This extremely good match between experiment and theory indicates not only that the *ab initio* geometry of methylamine ion is quite accurate, but also that a kinetic coupling may exist between internal rotations of the top and frame especially when those values

TABLE II. Molecular constants used in the simulations for $CH_3NH_2^+$ MATI spectra.

	Origin	ν_9^+	ν_7^+	$2\nu_9^+$	$\nu_7^+ + \nu_9^+$	$2\nu_7^+$	$3\nu_9^+$
A^T	(10.5)	(10.12)					
A^F	(5.25)	(5.06)					
B	(0.8)	(0.8)					
E_{vib}^+	0[+72930]	738±3	1013±3	1475±3	1749±5	2020±5	2219±10

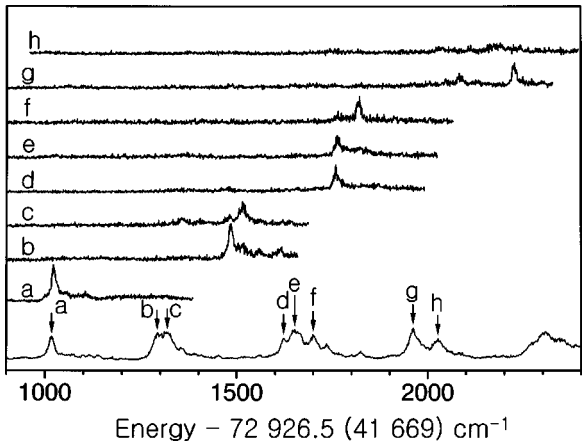

FIG. 10. MATI spectra of $CH_3NH_2^+$ taken via various intermediate states with internal energies above ~1000 cm^{-1} (Ref. 23). See the caption in Fig. 6.

are quite similar to each other. Vibrational frequencies of ν_9^+ and ν_7^+ of $CH_3NH_2^+$ ($CH_3ND_2^+$) are calculated to be 736.12 (577.48) and 1087.47 (1067.94) cm^{-1}, respectively, Table III. The calculated ν_9^+ frequencies are very close to the corresponding experimental values, while the calculation is a little bit higher than the experiment for the ν_7^+ frequency. The experimental ν_7^+ fundamental frequency of $CH_3ND_2^+$ is higher than that of $CH_3NH_2^+$, while *ab initio* calculation predicts the opposite. This is also observed in neutral excited methylamines in the preceding paper. Measurement of anharmonic coupling constants would be desirable for a better understanding. The zero-point energy difference between $CH_3NH_2^+$ and $CH_3ND_2^+$ is estimated to be 1298 cm^{-1} from their respective ionization energies of 72 930 and 73 019 cm^{-1} and the zero-point energy difference of 1387 cm^{-1} between neutral ground CH_3NH_2 and CH_3ND_2. The zero-point energy difference between $CH_3NH_2^+$ and $CH_3ND_2^+$ is calculated to be 1380 cm^{-1} from their *ab initio* vibrational frequencies, and this is in good agreement with the experiment. The reasonable experimental value of the zero-point energy difference between $CH_3NH_2^+$ and $CH_3ND_2^+$ confirms that the abnormally small experimental value for the zero-point energy difference between CH_3NH_2 and CH_3ND_2 in their neutral excited states is real.[23]

The thermodynamic properties of methylamine are important for understanding steric and/or electron-donating effects of alkyl groups on basicities of various amines.[1–5] Accordingly, many basic properties such as gas-phase basicity, proton affinity, and hydrogen atom affinity have been measured for many kinds of aliphatic amines for decades. Especially, it has been known that since the proton affinity (PA) and ionization potential (IP) change approximately in a parallel way so that the hydrogen atom affinity (HA) of a base ion (B^+), given as $HA(B^+)=IP(B)+PA(B)-IP(H)$, remains roughly constant for a series of related aliphatic

TABLE III. Geometry parameters and vibrational frequencies of methylamine cations in D_0 states [QCISD/6-31+G(d)].[a]

	$CH_3NH_2^+$		$CH_3ND_2^+$		
	Ab initio	Expt.	*Ab initio*	Expt.	Assignment
r_{CN}	1.438		1.438		
r_{CHa}	1.110		1.110		
r_{CHb}	1.094		1.093		
$r_{NH(D)c}$	1.027		1.027		
a_{HaCN}	107.120		107.120		
a_{HbCN}	109.787		109.787		
$a_{H(D)cNC}$	121.747		121.747		
a_{HaCHb}	108.439		108.439		
$d_{HaCNH(D)c}$	88.112		88.112		
$d_{HbCNH(D)c}$	−29.439		−29.439		
A^T	11.060	10.5	5.530	5.25	
A^F	5.198	5.25	5.198	5.25	
B	0.679		0.575		
a'	736.12	738	577.48	573	$NH(D)_2$ wag
a'	1010.79		957.27		CN str
a'	1087.47	1013	1067.94	1024	CH_3 rock
a'	1414.43		1413.58		CH_3 s-deform
a'	1505.59		1510.51		CH_3 d-deform
a'	1661.43		1259.66		$NH(D)_2$ scis
a'	2969.53		2969.50		CH_3 s-str
a'	3138.89		3138.89		CH_3 d-str
a'	3461.45		2503.27		$NH(D)_2$ s-str
a''	85.25		67.77		Torsion
a''	920.41		736.61		CH_3 rock
a''	1275.81		1213.59		$NH(D)_2$ twist
a''	1464.02		1457.69		CH_3 d-deform
a''	3213.36		3213.37		CH_3 d-str
a''	3573.69		2649.79		$NH(D)_2$ a-str

[a]See Fig. 3(a) for labeling of atoms.

amines.[1] The hydrogen atom affinity of methylamine (CH_3NH_2) had been estimated to be 104 kcal/mol, from its proton affinity and IP of 214.1 and 205 kcal/mol (8.89 eV), respectively, when an IP(H) of 315.1 kcal/mol was used.[1] The more recently measured value of the methylamine proton affinity, 214.9 kcal/mol,[5] does not change the value of methylamine HA significantly. However, the newly measured IP of methylamine, which is 208.5 kcal/mol (9.0422 eV), let the hydrogen atom affinity of methylamine (CH_3NH_2) be readjusted to ~107.5 kcal/mol.

IV. CONCLUSIONS

The ionization energies of methylamines (CH_3NH_2 and CH_3ND_2) are accurately and precisely determined to be 9.0422 ± 0.0012 and 9.0532 ± 0.0012 eV, respectively, by $(1+1)$ two-photon mass-analyzed threshold ionization spectroscopy. To our knowledge, this is the first report of precise ionization energies of methylamines, although the relatively less precise ionization potentials measured by photoelectron spectroscopy had been reported earlier.[6,7] Similar to the case of methylamines in 3*s* excited states, the amino moiety internally rotates nearly freely with respect to the methyl group along the C–N axis also in methylamine cations. Torsional barrier heights of $CH_3ND_2^+$ are 25 ± 5 and 34 ± 5 cm^{-1} at the origin and first ND_2-wagging bands, respectively. Fundamental frequencies of the amino-wagging and CH_3-rocking modes of $CH_3NH_2^+$ ($CH_3ND_2^+$) in D_0 states are determined to be 738 (573) and 1013 (1024) cm^{-1}, respectively. Internal-rotational constants are also quite accurately determined, from which geometries of methylamine ions are revealed. The *ab initio* [QCISD level with a 6-31+G(d) basis set] calculation is quite consistent with the experiment in terms of both geometric parameters and vibrational frequencies. Mode-resolved spectroscopy using the MATI signal is proven to be extremely powerful in resolving overlapped spectral features in the intermediate state. The thermodynamic properties of methylamines associated with their ionization energies are to be adjusted according to newly measured ionization energies here. Accordingly, the hydrogen atom affinity of methylamine (CH_3NH_2) is reestimated to be ~107.5 kcal/mol. One-photon vacuum–UV (VUV) MATI spectroscopy of methylamine would provide richer information about cationic vibrational modes other than amino wag and CH_3 rock. Especially, since one-photon ionization is a bound-to-bound transition, a mode such as N–H(D) stretching possibly missed in the $\tilde{A}-X$ transition may appear in the one-photon VUV MATI spectrum. Application of MATI or ZEKE spectroscopy to other various aliphatic amines will provide accurate ionization potentials of such important compounds, and those values would be extremely useful in investigating electric and/or steric effects of alkyl groups on amine basicities. This would contribute to a better understanding of amine chemistry, which is extremely important in chemistry and biology.

ACKNOWLEDGMENT

This work was financially supported by Korea Research Foundation Grant No. KRF-2002-070-C00046.

[1] *Gas Phase Ion Chemistry*, edited by M. T. Bowers (Academic, New York, 1979), and references therein.
[2] D. H. Aue, H. M. Webb, and M. T. Bowers, J. Am. Chem. Soc. **98**, 311 (1976).
[3] M. T. Bowers, D. H. Aue, H. M. Webb, and R. T. McIver, J. Am. Chem. Soc. **93**, 4314 (1971).
[4] D. C. Caskey, R. Damrauer, and D. McGoff, J. Org. Chem. **67**, 5098 (2002), and references therein.
[5] E. P. Hunter and S. G. Lias, J. Phys. Chem. Ref. Data **27**, 413 (1998).
[6] K. Kimura, S. Katsumata, Y. Achiba, T. Yamazaki, and S. Iwata, *Handbook of He I Photoelectron Spectra of Fundamental Organic Molecules* (Japan Scientific Societies, Tokyo, 1981).
[7] Z. F. Hu, Z. Y. Wang, X. L. Kong *et al.*, Acta Phys. Sin. **51**, 235 (2002).
[8] E. W. Schlag, *ZEKE Spectroscopy* (Cambridge University Press, Cambridge, England, 1998), and references therein.
[9] K. Müller-Dethlefs and E. W. Schlag, Annu. Rev. Phys. Chem. **42**, 109 (1991).
[10] K. Müller-Dethlefs, M. Sander, and E. W. Schlag, Chem. Phys. Lett. **112**, 291 (1984).
[11] I. Fischer, R. Lindner, and K. Müller-Dethlefs, J. Chem. Soc., Faraday Trans. **90**, 2425 (1994).
[12] L. Zhu and P. Johnson, J. Chem. Phys. **94**, 5769 (1991).
[13] H. Krause and H. J. Neusser, J. Chem. Phys. **97**, 5923 (1992).
[14] S. T. Park, S. K. Kim, and M. S. Kim, Nature (London) **415**, 306 (2002).
[15] S. T. Park, S. K. Kim, and M. S. Kim, J. Chem. Phys. **114**, 5568 (2001).
[16] J. W. Hepburn, Chem. Soc. Rev. **25**, 281 (1996).
[17] K. Kimura, J. Electron Spectrosc. Relat. Phenom. **100**, 273 (1999).
[18] D. Lee, S. J. Baek, K.-W. Choi, Y. S. Choi, and S. K. Kim, Bull. Korean Chem. Soc. **23**, 277 (2002).
[19] S. J. Baek, K.-W. Choi, Y. S. Choi, and S. K. Kim, J. Chem. Phys. **117**, 2131 (2002).
[20] M. Takahashi, H. Ozeki, and K. Kimura, J. Chem. Phys. **96**, 6399 (1992).
[21] X. Zhang, J. M. Smith, and J. L. Knee, J. Chem. Phys. **97**, 2843 (1992).
[22] X. Song, M. Yang, E. R. Davidson, and J. P. Reilly, J. Chem. Phys. **99**, 3224 (1993).
[23] S. J. Baek, K.-W. Choi, Y. S. Choi, and S. K. Kim, J. Chem. Phys. **118**, 11026 (2003), preceding paper.